PHYSICAL REVIEW B **87**, 121201(R) (2013)

Bragg x-ray ptychography of a silicon crystal: Visualization of the dislocation strain field and the production of a vortex beam

Yukio Takahashi,[1,*] Akihiro Suzuki,[1] Shin Furutaku,[1] Kazuto Yamauchi,[1] Yoshiki Kohmura,[2] and Tetsuya Ishikawa[2]

[1]*Graduate School of Engineering, Osaka University, 2-1 Yamada-oka, Suita, Osaka 565-0871, Japan*

[2]*RIKEN SPring-8 Center, 1-1-1 Kouto, Sayo-cho, Sayo, Hyogo 679-5148, Japan*

(Received 19 April 2012; revised manuscript received 10 September 2012; published 7 March 2013)

We experimentally demonstrate the visualization of nanoscale dislocation strain fields in a thick silicon single crystal by a coherent diffraction imaging technique called Bragg x-ray ptychography. We also propose that the x-ray microbeam carrying orbital angular momentum is selectively produced by coherent Bragg diffraction from dislocation singularities in crystals. This work not only provides us with a tool for characterizing dislocation strain fields buried within extended crystals but also opens up new scientific opportunities in femtosecond spectroscopy using x-ray free-electron lasers.

DOI: 10.1103/PhysRevB.87.121201 PACS number(s): 61.72.Hh, 42.30.−d, 07.85.Tt, 41.50.+h

Dislocations, i.e., topological line defects in a crystal lattice, have characteristic strain fields, which are of considerable importance in many areas of materials science.[1] They are well known to be responsible for plastic behavior and also affect the electronic properties of materials. Extended phase objects such as dislocations embedded in materials are usually observed by transmission electron microscopy (TEM)[2] or x-ray topography.[3] However, electron microscopy is restricted to thin samples and x-ray topography has limited resolution. The nondestructive and high-resolution observation of dislocation strain fields buried within a bulk specimen is a remaining task in microscopy. Dislocations also play a crucial role in optics. One generally describes light rays as plane waves, i.e., as a light beam with a constant phase that extends infinitely perpendicular to the Poynting vector. Light rays exist for which both the intensity perpendicular to the propagation direction of the light and the phase of the light vary. One can even create light rays, in which the phase of the light shows a singularity, a so-called vortex.[4] The realization of vortex beams formed from x rays[5,6] and electrons[7] has been experimentally demonstrated. Such vortex beams can carry orbital angular momentum (OAM), enabling their use in various types of novel spectroscopy measurements.[8,9] Thus, the visualization of dislocation strain fields and the generation of vortex beams are closely related and are now a rich and diverse topic of fundamental and applied research.

Coherent x rays are a promising light for probing the dislocation strain fields in bulk specimens and for producing vortex beams with a short wavelength. Up to now, misfit[10] and charge-density-wave dislocations,[11] as well as the dissociation of bulk dislocations,[12] have been studied by means of coherent x-ray diffraction at synchrotron radiation facilities. The goal of the coherent diffraction technique is to obtain real-space images of samples from measured diffraction intensities, which is called coherent diffraction imaging (CDI).[13,14] CDI originated from the desire to extend the ideas of crystallography to nonperiodic samples. However, CDI is also suited for the study of strained crystals in Bragg geometry,[15] in which the retrieved phase information corresponds to the strain within a crystal. Bragg CDI allows us to obtain very high resolution three-dimensional images of strain within nanocrystals. Recently, Bragg CDI based on a scanning method[16,17] has been demonstrated, which is known as "Bragg ptychography,"[18] in which a probe is scanned across a sample and the coherent Bragg diffraction pattern is observed at each beam position. Bragg ptychography is a promising technique for visualizing the dislocation strain fields in extended crystals.

In this Rapid Communication, we report the quantitative visualization of nanoscale dislocation strain fields in a thick silicon single crystal by Bragg x-ray ptychography. We retrieve the wave front containing the x-ray vortex using coherent Bragg diffraction from the dislocations inside the crystal.

The experiment on Bragg x-ray ptychography was carried out at BL29XUL (Ref. 19) in SPring-8. Figure 1 shows a schematic of the experimental setup. The apparatus was set up in a constant-temperature room to suppress thermal drift. The temperature change in the experimental hutch was controlled to less than 0.1 K during the measurement. A 11.8 keV monochromatic x-ray beam (wavelength $\lambda = 0.1051$ nm) was generated by an in-vacuum undulator device and a Si(111) double-crystal monochromator (energy bandwidth of $\sim 1.3 \times 10^{-4}$), resulting in a longitudinal coherence length of ~ 1 μm. The monochromatic x-ray beam was two-dimensionally focused to a ~ 1 μm spot size using Kirkpatrick-Baez (KB) mirror optics placed ~ 47 m downstream from a virtual source of 10 μm square. The flux of the focused x rays was estimated to be $\sim 3 \times 10^7$ photons/s. The sample was a single-crystal (100)-oriented silicon membrane of 1-μm thickness, which was purchased from Norcada Inc. (Edmonton, Canada). The silicon membrane was produced by the chemical etching of a bonded silicon-on-insulator (SOI) wafer. It has previously been reported that two types of periodic dislocation are localized at the bonding interface of an SOI wafer.[20] These dislocations should remain on the surface of the present silicon membrane. 220 coherent Bragg diffraction patterns were measured in a nearly symmetrical Laue geometry. The extinction length l_L was ~ 33 μm, which is about ten times more than the sample thickness, and hence the multiple-scattering effect was negligible in our experiment. The maximum variation of the x-ray path length in the sample was 0.55 μm when the beam size is defined as the size of the main beam of 1 μm, which is less than the longitudinal coherence length. In addition, the absorption of the incident x rays was less than 1%, and hence the effect of absorption can be ignored.

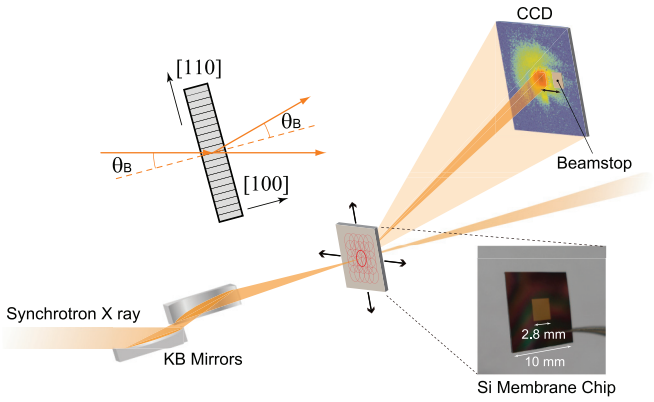

FIG. 1. (Color online) Schematic view of ptychographic hard x-ray Bragg diffraction microscope. X rays with energy of 11.8 keV were two-dimensionally focused to an ~ 1 μm spot size using KB mirrors. The 1-μm-thick silicon single-crystal membrane was located on the focal plane and was mounted on a multiaxis sample stage. The sample position was precisely controlled using piezo stages with capacitive sensors. 220 Bragg diffraction intensities (Bragg angle $\theta_B = 15.88^\circ$) were detected using a CCD detector with a pixel size of 20×20 μm^2, which was positioned at a distance of 2 m from the sample. The sample was illuminated in 20×20 overlapping fields of view that were separated by 500 and 520 nm in the horizontal and vertical directions, respectively. Owing to the large dynamic range of the coherent diffraction intensity across the frequency spectrum, the 400 ptychographic diffraction patterns were separately measured to obtain diffraction data with and without the Bragg peak.

The coherent Bragg diffraction patterns were recorded with an x-ray direct-detection charge-coupled device (CCD). The x-ray exposure time at each position was 10.3 s. It took ~ 6 h to collect the 400 ptychographic diffraction patterns in a 20×20 overlapping field, which includes the readout time from the CCD and the beamstop motion at each position.

Figure 2(a) shows a series of measured coherent Bragg diffraction patterns obtained from the silicon membrane, which are displayed on a log scale. Figure 2(b) shows three typical images labeled A, B, and C in Fig. 2(a). The highly intense region at the center of each image is displayed on a linear scale in the lower right. Pattern A shows the coherent diffraction obtained in a perfect region of the sample. The square shape of the Bragg spot at the center reflects the shape of the aperture immediately before the mirror. The upper and lower streaks are the tails of the Fresnel diffraction from the square aperture before the mirrors. Patterns B and C show the coherent Bragg diffraction from regions including a dislocation. In particular, many patterns similar to pattern B were observed in the sample. The Bragg spot in pattern B is divided into two parts, which is due to the dislocation-induced destructive interference at the position of Bragg reflection.[12] On the other hand, the Bragg spot in pattern C has a hollow structure with negligible intensity at its center.

The wave exiting the specimen in the direction of the Bragg diffracted beam propagates to the far field, where the intensity is recorded with the CCD detector. At the jth scan point, the measured intensity of the diffraction pattern is

$$I_j(\mathbf{q}) = |\mathcal{F}[P(\mathbf{r} - \mathbf{r}_j)O_B(\mathbf{r})]|^2, \qquad (1)$$

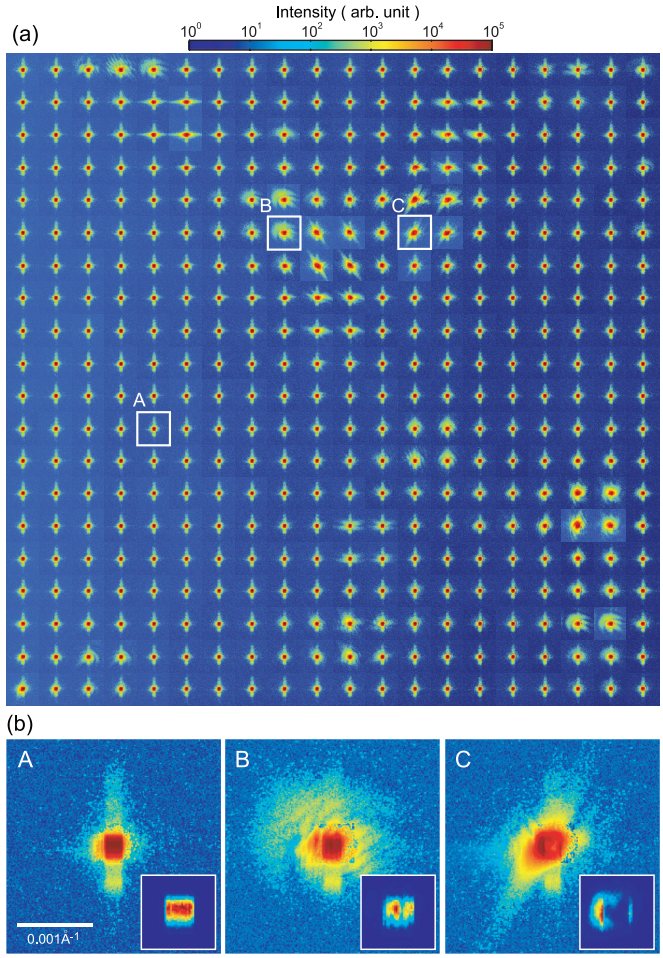

FIG. 2. (Color online) (a) Coherent Bragg diffraction patterns (log scale) of 220 reflection of the silicon membrane with 500×520 nm^2 steps. Each pattern is composed of an array of 301×301 pixels and its pixel resolution is 9.52×10^{-6} Å^{-1}. (b) Enlarged images of diffraction patterns labeled in (a). The central 41×41 pixels are displayed in the lower right on a linear scale.

where $\mathcal{F}$ is the Fourier transform operation with the two-dimensional reciprocal space coordinate $\mathbf{q}$, P is the probe function, $\mathbf{r}_j$ is the scanning position, and O_B is the complex function of the object under the Bragg condition. O_B is expressed as

$$O_B(\mathbf{r}) = |O_B(\mathbf{r})|\exp[i\{\phi_s(\mathbf{r}) + \phi_r(\mathbf{r})\}], \qquad (2)$$

where ϕ_s and ϕ_r are the phase shifts due to the strain field and optical reflection, respectively. In our experiment, the optical path length of x rays in the sample is almost uniform because of the nearly symmetrical Laue geometry and the constant thickness of the sample. Therefore, ϕ_r was almost uniform.

Both the complex function of the object and the complex illuminating wave field were reconstructed from the 400 diffraction patterns using the extended ptychographical iterative algorithm.[21] The reconstruction started from an initial Gaussian wave field and a flat object with a constant transmissivity and without phase shift. The iterative process was continued for up to 5×10^2 iterations. Figure 3(a) shows the reconstructed norm and phase of the locally averaged local crystal structure factor with a pixel size of 35.4 nm and a field

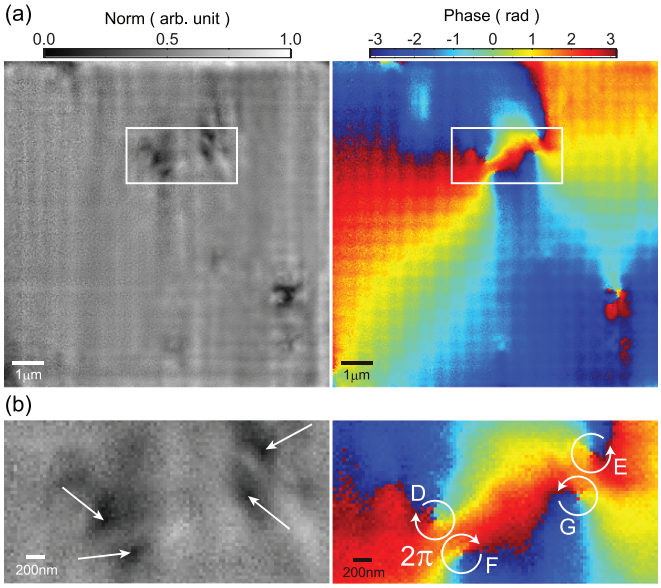

FIG. 3. (Color online) (a) Norm (left) and phase (right) maps of the locally averaged local crystal structure factor reconstructed from the ptychographic diffraction patterns in Fig. 2(a). The pixel size is 35.4 nm and the total number of pixels is 294 × 294. (b) Enlarged norm and phase maps of the area indicated by the square in (a).

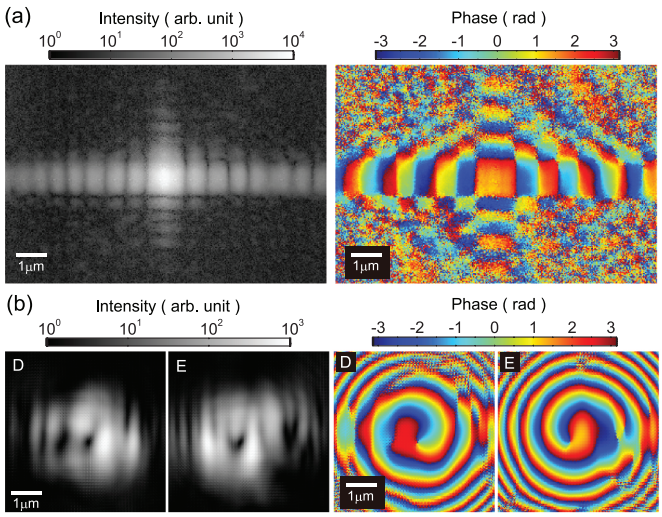

FIG. 4. (Color online) (a) Transverse profile of the reconstructed wave field at the focal plane of the focused x-ray beam. (b) Transverse profile of calculated x-ray wave field 10 mm downstream from the sample when the focused x-ray beam is irradiated to the vortex cores of D and E in Fig. 3(b).

of view of $\sim 10 \times 10\ \mu\text{m}^2$. The periodic pattern is an artifact due to the translation symmetry of the raster scan. In addition to the artifact, distinct contrast due to the dislocation strain field exists in the reconstructed image where the intensity is low and the phase shift is steep. Figure 3(b) shows an enlarged image of the area surrounded by the white square in Fig. 3(a). It is noteworthy that there are four screw-type phase singularities, which appear to be two pairs of vortices with opposite directions (i.e., D-E and F-G). The singularities correspond to the local minimum positions in the intensity image, which are shown by the white arrows in Fig. 3(b). It is considered that two dislocation loops exist in the (111) plane. The (110) plane crosses the dislocation loops, producing a pair of vortices with opposite directions in the (110) plane. The directions of the Burgers vectors of the dislocation loops are opposite each other, which results in the opposite vortex directions of the loops. The diameter of each loop and the distance between the loops are estimated to be approximately 1–2 μm and $\sim$200 nm, respectively, from the reconstructed image.

TEM and x-ray topography are well-established tools for the observation of dislocation strain fields, in which the dislocations are imaged on the basis of the diffraction contrast from them. Although TEM can image the nanometer-scale dislocation of thin samples, the interpretation of the contrast of thick samples is difficult because the multiple scattering and inelastic scattering of the electrons should be considerable. X-ray topography can probe bulk dislocations but with a much poorer resolution, in which the spatial resolution is limited by the resolution of the detector, the experimental geometry, and intrinsic diffraction effects. On the other hand, Bragg x-ray ptychography can overcome the limitation of the spatial resolution of x-ray topography because the spatial resolution is limited by only diffraction effects. The spatial resolution in the present Bragg x-ray ptychography is estimated to be $\sim$50 nm from both the coherent Bragg diffraction patterns and the reconstructed image, which is much better than x-ray topography. For unit incident intensity, the diffracted intensity from dislocations is approximately $(Dx/l_L)^2$, where D_x is structural resolution for dislocations, which is estimated to be $\sim 2 \times 10^{-6}$ in the present results. Thus, the spatial resolution of Bragg x-ray ptychography is practically limited by the flux of the coherent x rays, which will be improved by using the high-brilliant next-generation x-ray sources. In addition, the field of view (FOV) as well as the spatial resolution is an important factor for microscopy. FOV is $\sim 10 \times 10\ \mu\text{m}^2$ in the present result, which is less than 1/100 of x-ray topography. Therefore, Bragg x-ray ptychography and x-ray topography should be complementary methods in the spatial scale for the observation of dislocation strain fields buried within thick samples.

Figure 4(a) shows transverse profiles of reconstructed illumination wave field. The intensity and phase distributions are similar to those of Fraunhofer diffraction from a rectangular aperture. Both the main peak and the high-order fringes are clearly visible. The highest-order spots are observed at a distance of $\sim 2\ \mu$m in the vertical direction and $\sim 4\ \mu$m in the horizontal direction from the main peak and have an intensity of $\sim$1/1000 of the main peak. The reconstruction of the high-order diffraction spots with low intensity implies that the positioning error due to the drift was small and that reliable reconstruction was carried out. The period of the fringe in the vertical direction is shorter than that in the horizontal direction, which results from the small gap under the Bragg condition in the present experiment. The low signal-to-noise ratio of the fringe in the vertical direction is due to the poor longitudinal coherence. Figure 4(b) shows transverse profiles of the wave field 10 mm downstream from the sample, which was calculated using the angular spectrum method,[22] when the focused x-ray beam is irradiated to the vortex cores of

D and E. Note that x-ray vortex beams with a characteristic hollow profile and helical phase are derived. The two vortices correspond to the $l = \pm 1$ modes, where l is the azimuthal mode index. These spiral directions correspond to the rotational directions of the phase singularities at D and E in Fig. 3(b). Higher-order diffractions such as (440) should generate x-ray vortex beams with $|l| \geqslant 2$. Thus, one can select the dislocation cores based on the strain map and then control the OAM mode. This is a significant advantage for the generation of x-ray vortex beams.

In conclusion, we have visualized the dislocation strain fields of a thin Si single crystal by Bragg ptychography using a highly focused hard x-ray beam. The present coherent method allows one to quantitatively characterize the strain distribution of various extended crystals such as epitaxial thin films or polycrystalline materials, and should be a complementary method with x-ray topography and electron microscopy. Although only a projection image of the dislocation strain fields was visualized in the present study, three-dimensional dislocation strain fields will be visualized by precisely controlling the detuning angle of the main crystal from the exact Bragg position and collecting the diffraction data at many detuning angles. This should further our understanding of the electronic and mechanical properties linking the spatial distribution of local strains at a large scale and their interaction. We have also proposed the generation of x-ray vortex microbeams using coherent Bragg diffraction from dislocation singularities in a thin silicon crystal. A significant advantage of this method is that one can switch the OAM mode by selecting the dislocation singularity and diffraction index. Strong dichroic effects induced by an x-ray beam with OAM have been predicted,[9] which will help provide a clear description of quadrupolar transitions and the magnetism of $3d$ transition-metal systems. Recently, a scheme to generate intense coherent light with OAM at the fundamental wavelength of an x-ray free-electron laser (XFEL) has been proposed.[23] A thin silicon crystal is useful for XFEL vortex optics because of its low x-ray absorption. An XFEL with OAM will open up new frontiers of femtosecond spectroscopy in the fields of orbital physics and magnetism.

This work was supported by a Grants-in-Aid for Scientific Research (Grants No. 24651137 and No. 23102504), the Global COE Program "Center of Excellence for Atomically Controlled Fabrication Technology," and X-ray Free Electron Laser Priority Strategy Program from the Ministry of Education, Culture, Sports, Science and Technology.

*Corresponding author: takahashi@prec.eng.osaka-u.ac.jp

[1] *Dislocation in Solids*, edited by F. R. N. Nabarro and M. S. Duesbery, Vols. 1–11 (Amsterdam, North Holland, 1979–2003).

[2] C. T Forwood and L. M Clarebrough, *Electron Microscopy of Interfaces in Metals and Alloys* (Adam Hilger, London, 1991).

[3] B. K. Tanner, *X-ray Diffraction Topography* (Pergamon, Oxford, 1976).

[4] L. Allen, M. W. Beijersbergen, R. J. C. Spreeuw, and J. P. Woerdman, Phys. Rev. A **45**, 8185 (1992).

[5] A. G. Peele, P. J. McMahon, D. Paterson, C. Q. Tran, A. P. Mancuso, K. A. Nugent, J. P. Hayes, E. Harvey, B. Lai, and I. McNulty, Opt. Lett. **27**, 1752 (2002).

[6] Y. Kohmura, K. Sawada, M. Taguchi, T. Ishikawa, T. Ohigashi, and Y. Suzuki, Appl. Phys. Lett. **94**, 101112 (2009).

[7] M. Uchida and A. Tonomura, Nature (London) **464**, 737 (2010).

[8] J. Verbeeck, H. Tian, and P. Schattschneider, Nature (London) **467**, 301 (2010).

[9] M. van Veenendaal and I. McNulty, Phys. Rev. Lett. **98**, 157401 (2007).

[10] I. K. Robinson, Y. Da, T. Spila, and J. E. Greene, J. Phys. D: Appl. Phys. **38**, A7 (2005).

[11] D. Le Bolloc'h, S. Ravy, J. Dumas, J. Marcus, F. Livet, C. Detlefs, F. Yakhou, and L. Paolasini, Phys. Rev. Lett. **95**, 116401 (2005).

[12] V. L. R. Jacques, S. Ravy, D. Le Bolloc'h, E. Pinsolle, M. Sauvage-Simkin, and F. Livet, Phys. Rev. Lett. **106**, 065502 (2011).

[13] H. N. Chapman and K. A. Nugent, Nat. Photonics **4**, 833 (2010).

[14] J. Miao, P. Charalambous, J. Kirz, and D. Sayre, Nature (London) **400**, 342 (1999).

[15] I. K. Robinson and R. Harder, Nature Mater. **8**, 291 (2009).

[16] J. M. Rodenburg, A. C. Hurst, A. G. Cullis, B. R. Dobson, F. Pfeiffer, O. Bunk, C. David, K. Jefimovs, and I. Johnson, Phys. Rev. Lett. **98**, 034801 (2007).

[17] P. Thibault, M. Dierolf, A. Menzel, O. Bunk, C. David, and F. Pfeiffer, Science **321**, 379 (2008).

[18] P. Godard, G. Carbone, M. Allain, F. Mastropietro, G. Chen, L. Capello, A. Diaz, T. H. Metzger, J. Stangl, and V. Chamard, Nat. Commun. **2**, 568 (2011).

[19] K. Tamasaku, Y. Tanaka, M. Yabashi, H. Yamazaki, N. Kawamura, M. Suzuki, and T. Ishikawa, Nucl. Instrum. Methods Phys. Res. A **467**, 686 (2001).

[20] J. Eymery, D. Buttard, F. Fournel, H. Moriceau, G. T. Baumbach, and D. Lubbert, Phys. Rev. B **65**, 165337 (2002).

[21] A. M. Maiden and J. M. Rodenburg, Ultramicroscopy **109**, 1256 (2009).

[22] J. W. Goodman, *Introduction to Fourier Optics*, 2nd ed. (McGraw-Hill, New York, 1996), Chap. 3.

[23] E. Hemsing, A. Marinelli, and J. B. Rosenzweig, Phys. Rev. Lett. **106**, 164803 (2011).